Experimental observation of the quantum speed limit as the true evolution time

Ben Wang,[1] Qianyi Wang,[1] Huai-Ming Yu,[2] Liang Xu,[1,*] Jing Liu,[2,†] and Lijian Zhang[1,‡]

[1]National Laboratory of Solid State Microstructures,
Key Laboratory of Intelligent Optical Sensing and Manipulation, College of Engineering and Applied Sciences,
and Collaborative Innovation Center of Advanced Microstructures, Nanjing University, Nanjing 210093, China
[2]Center for Theoretical Physics and School of Physics and Optoelectronic Engineering,
Hainan University, Haikou, Hainan 570228, China

S1. THE OPERATION OF HWP AND QWP

Half-wave plates (HWPs) and quarter-wave plates (QWPs) are commonly used to manipulate the polarization state of photons. In our experiment, we consider a basis consisting of horizontal polarization state ($|H\rangle$) and vertical polarization state ($|V\rangle$), which can be represented as:

$$|H\rangle = \begin{pmatrix} 1 \\ 0 \end{pmatrix}, \qquad |V\rangle = \begin{pmatrix} 0 \\ 1 \end{pmatrix}. \tag{1}$$

Under this basis, The corresponding representation of HWP and QWP are given by:

$$\mathrm{HWP}(\theta_H) = \begin{pmatrix} \cos 2\theta_H & \sin 2\theta_H \\ \sin 2\theta_H & -\cos 2\theta_H \end{pmatrix}, \qquad \mathrm{QWP}(\theta_Q) = \begin{pmatrix} \cos^2\theta_Q + i\sin^2\theta_Q & (1-i)\sin\theta_Q\cos\theta_Q \\ (1-i)\sin\theta_Q\cos\theta_Q & i\cos^2\theta_Q + \sin^2\theta_Q \end{pmatrix}, \tag{2}$$

where θ_H and θ_Q represent the angles between the optical axes of the waveplates and the direction of horizontal polarization.

It is worth noting that any unitary evolution can be realized by placing an HWP between two QWPs, forming a configuration commonly referred to as QHQ. A common setting for QHQ is to have the two QWPs set at 45° and the corresponding matrix of this kind of QHQ is

$$U_{\mathrm{QHQ}}(\theta_H) = \begin{pmatrix} e^{i(-2\theta_H + \frac{\pi}{2})} & 0 \\ 0 & e^{i(2\theta_H - \frac{\pi}{2})} \end{pmatrix}. \tag{3}$$

where θ_H represents the angle of the HWP. The function of this QHQ configuration on the horizontally polarized state and vertically polarized state can be easily derived as

$$U_{\mathrm{QHQ}}(\theta_H)|H\rangle = ie^{-i2\theta_H}|H\rangle, \qquad U_{QHQ}(\theta_H)|V\rangle = -ie^{i2\theta_H}|V\rangle. \tag{4}$$

S2. QUTRIT SYSTEM

SU(3) generators

The generators of SU(3) used in our paper are

$$\begin{aligned}
\lambda_1 &= \begin{pmatrix} 0 & 1 & 0 \\ 1 & 0 & 0 \\ 0 & 0 & 0 \end{pmatrix}, \quad \lambda_2 = \begin{pmatrix} 0 & 0 & 1 \\ 0 & 0 & 0 \\ 1 & 0 & 0 \end{pmatrix}, \\
\lambda_3 &= \begin{pmatrix} 0 & 0 & 0 \\ 0 & 0 & 1 \\ 0 & 1 & 0 \end{pmatrix}, \quad \lambda_4 = \begin{pmatrix} 0 & -i & 0 \\ i & 0 & 0 \\ 0 & 0 & 0 \end{pmatrix}, \\
\lambda_5 &= \begin{pmatrix} 0 & 0 & -i \\ 0 & 0 & 0 \\ i & 0 & 0 \end{pmatrix}, \quad \lambda_6 = \begin{pmatrix} 0 & 0 & 0 \\ 0 & 0 & -i \\ 0 & i & 0 \end{pmatrix}, \\
\lambda_7 &= \begin{pmatrix} 1 & 0 & 0 \\ 0 & -1 & 0 \\ 0 & 0 & 0 \end{pmatrix}, \quad \lambda_8 = \frac{1}{\sqrt{3}} \begin{pmatrix} 1 & 0 & 0 \\ 0 & 1 & 0 \\ 0 & 0 & -2 \end{pmatrix}.
\end{aligned} \tag{5}$$

TABLE I: Waveplate setting angles for different projective measurements in qutrit system.

states	QWP$_1$(°)	HWP$_1$(°)	QWP$_2$(°)	HWP$_2$(°)
$\|0\rangle$	0	0	0	0
$\|1\rangle$	0	45	0	0
$\|2\rangle$	0	0	0	45
$\frac{1}{\sqrt{2}}(\|0\rangle+\|1\rangle)$	45	22.5	0	0
$\frac{1}{\sqrt{2}}(\|0\rangle-\|1\rangle)$	45	-22.5	0	0
$\frac{1}{\sqrt{2}}(\|0\rangle+i\|1\rangle)$	0	-22.5	0	0
$\frac{1}{\sqrt{2}}(\|0\rangle-i\|1\rangle)$	0	22.5	0	0
$\frac{1}{\sqrt{2}}(\|0\rangle+\|2\rangle)$	0	0	45	45
$\frac{1}{\sqrt{2}}(\|0\rangle-\|2\rangle)$	0	0	45	0
$\frac{1}{\sqrt{2}}(\|0\rangle+i\|2\rangle)$	0	0	45	22.5
$\frac{1}{\sqrt{2}}(\|0\rangle-i\|2\rangle)$	0	0	45	-22.5
$\frac{1}{\sqrt{2}}(\|1\rangle+\|2\rangle)$	0	45	45	-22.5
$\frac{1}{\sqrt{2}}(\|1\rangle-\|2\rangle)$	0	45	45	22.5
$\frac{1}{\sqrt{2}}(\|1\rangle+i\|2\rangle)$	0	45	0	22.5
$\frac{1}{\sqrt{2}}(\|1\rangle-i\|2\rangle)$	0	45	0	-22.5

TABLE II: Wave plate setting angles for different projective measurements in qubit system.

states	QWP$_3$(°)	HWP$_3$(°)
$\|0\rangle$	0	0
$\|1\rangle$	0	45
$\frac{1}{\sqrt{2}}(\|0\rangle+\|1\rangle)$	45	22.5
$\frac{1}{\sqrt{2}}(\|0\rangle-\|1\rangle)$	45	-22.5
$\frac{1}{\sqrt{2}}(\|0\rangle+i\|1\rangle)$	0	-22.5
$\frac{1}{\sqrt{2}}(\|0\rangle-i\|1\rangle)$	0	22.5

Measurement of qutrit

According to Born's rule, the probability of obtaining a state $|u\rangle$ when measuring a quantum system in the state $|\psi\rangle$ is given by $p = |\langle u|\psi\rangle|^2$. If we apply an unitary transformation U to $|\psi\rangle$,the probability of obtaining a state $|v\rangle$ is $p' = |\langle v|U|\psi\rangle|^2$. Therefore, if $|v\rangle = U|u\rangle$, then p' equals to p. This indicates that in order to determine the probability of obtaining $|u\rangle$ when measuring a $|\psi\rangle$, we can first apply an unitary operation U to the original state and then perform a projective measurement of $U|u\rangle$ in the final state.

In the measurement module, we first employ a BD to transform the optical path state into the polarization state. Then a unitary operation is applied to the polarization state by waveplates. Finally, we use BDs to transform the polarization state back to the path state. By this means, we can realize a unitary transformation to the qutrit state encoded in optical path modes. Since the detector is located in the top path of the qutrit, our implementation should transform the basis state $|u\rangle$ which we want the system to project into to top path. This ensures that the projective measurement of $|u\rangle$ under the original qutrit state is equivalent to the projective measurement of top path under the transformed qutrit state. The waveplate settings for different basis states are listed in Table I.

S3. OPEN QUBIT SYSTEM

Measurement of qubit

Similar to the discussion of the qutrit system, if we want to determine the probability of observing a specific state $|u\rangle$ under the original state, we need to transform the photons in $|u\rangle$ into the middle path where the detector is located. For projective measurement of different basis states, the settings of waveplates are listed in Table. II

S4. METHODS FOR STATE RECONSTRUCTION

We adopted the maximum likelihood technique as stated in Ref .[1] to reconstruct quantum states. The core idea of this method is to find a legal density matrix, parameterized by a set of parameters, that is most likely to yield the observed measurement counts. For a density matrix with dimension d, we adopt the following parameterization to make sure the density matrix remains legal for any parameters :

$$\rho(\boldsymbol{t}) = \frac{T^\dagger(\boldsymbol{t})T(\boldsymbol{t})}{\mathrm{Tr}[T^\dagger(\boldsymbol{t})T(\boldsymbol{t}))]}, \tag{6}$$

where $\boldsymbol{t}$ is a real vector with dimension equals to d^2 and $T(\boldsymbol{t})$ has the following tri-diagonal form:

$$T(\boldsymbol{t}) = \begin{pmatrix} t_1 & 0 & \dots & 0 \\ t_{d+1} + it_{d+2} & t_2 & \dots & 0 \\ \dots & \dots & \dots & 0 \\ t_{d^2-2d+3} + it_{d^2-2d+4} & t_{d^2-2d+5} + it_{d^2-2d+6} & \dots & t_d \end{pmatrix}. \tag{7}$$

Clearly, a matrix of this form satisfies the properties required for a density matrix, i.e. positive semidefinite, Hermitian and normalized. The likelihood function we utilize for the reconstruction is given by:

$$\mathcal{L}(\boldsymbol{t}) = \sum_r \frac{(\bar{n}_r - n_r(\boldsymbol{t}))^2}{2\bar{n}_r}, \tag{8}$$

where $n_r = \mathrm{Tr}(T^\dagger(\boldsymbol{t})T(\boldsymbol{t})|u_r\rangle\langle u_r|)$ and $|u_r\rangle$ represents the state for the projective measurement. $\bar{n}_r$ is the count of photons which are projected into $|u_r\rangle$ in our experiment. By minimizing the likelihood function, we can obtain an estimation of the density matrix that best matches our measurements. We assume this estimation is equal to the state we want to reconstruct.

S5. EXPERIMENTAL RESULTS OF ALL SELECTED STATES WITH FIXED PURITY

We show the results of 5 states of all states in the main text figure 4. Here, we show the experimental results of all selected states with fixed purity 0.855 in Fig. (S1).

To show the correctness of our experiments, we calculate the average fidelity of each initial state, $\mathcal{F}_{\mathrm{ave}} = \sum_i \mathcal{F}(\rho_{\exp}(t_i), \rho_{\mathrm{theory}}(t_i))$. The results is also shown in Fig. (S1).

S6. SIMULATION OF STATE PREPARATION ERRORS

To quantify the impact of imperfections in state preparation, we modeled an imperfect state, ρ_{error}, and calculated its effect on the target time required to reach a target angle of $2\pi/3$. The imperfect state is defined as:

$$\rho_{\mathrm{error}} = \frac{3\delta+1}{2}|\psi_1\rangle\langle\psi_1| + \frac{1-3\delta}{2}|\psi_2\rangle\langle\psi_2|, \tag{9}$$

where:

$$|\psi_1\rangle = \frac{1}{Z_1}\left(|0\rangle + (1+\eta_1)e^{i\phi_1}|1\rangle + (1+\eta_2)e^{i\phi_2}|2\rangle\right),$$
$$|\psi_2\rangle = \frac{1}{Z_2}\left(|0\rangle - (1+\eta_1)e^{i\phi_1}|1\rangle + (1+\eta_2)e^{i\phi_2}|2\rangle\right),$$

and Z_1, Z_2 are normalization factors. The parameters η_1, η_2 follow a normal distribution with mean 0 and standard deviation 0.05, representing amplitude errors, while ϕ_1, ϕ_2 follow a normal distribution with mean 0 and standard deviation 0.05π, representing phase errors.

When $\eta_1 = \eta_2 = \phi_1 = \phi_2 = 0$, ρ_{error} reduces to the ideal state:

$$\rho_{\mathrm{qt}}(\delta) = \begin{pmatrix} \frac{1}{3} & \delta & \frac{1}{3} \\ \delta & \frac{1}{3} & \delta \\ \frac{1}{3} & \delta & \frac{1}{3} \end{pmatrix}. \tag{10}$$

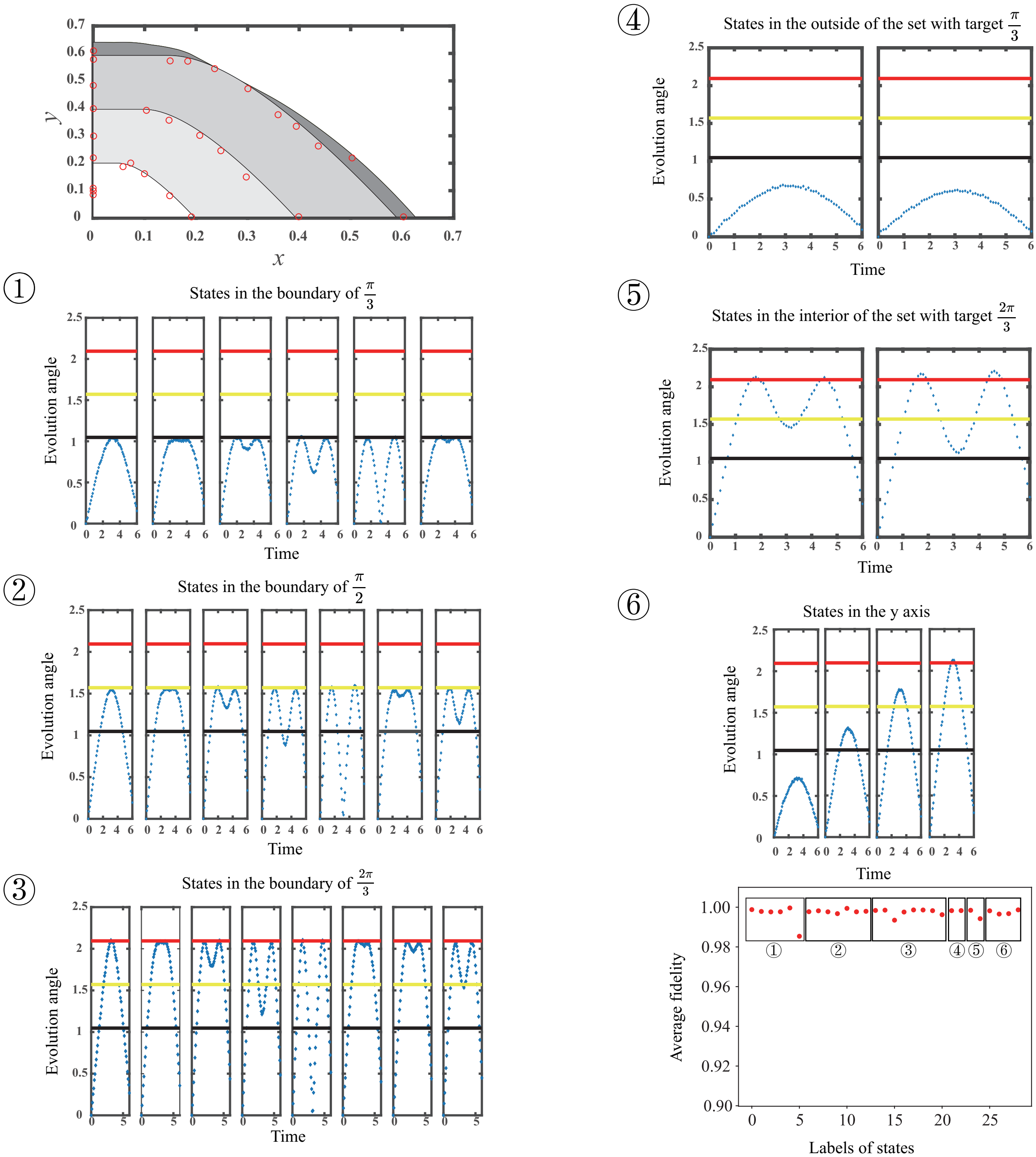

FIG. S1: The shapes of the reachable sets with fixed purity and the evolution angles of these initial state changes with evolution time. The average fidelity is shown in the last subfigure.

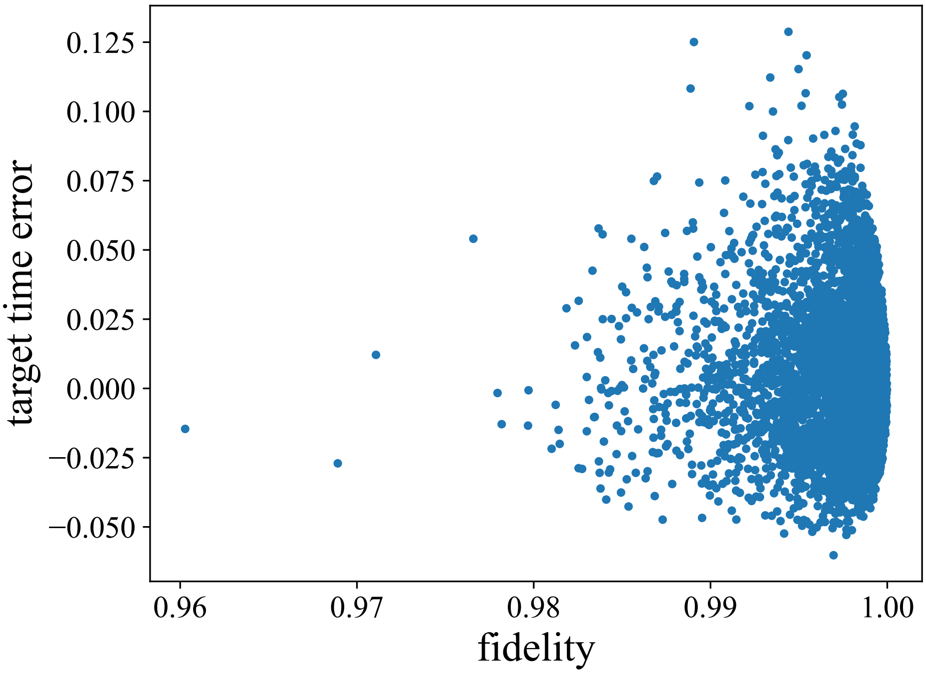

FIG. S2: Simulation results showing the impact of state preparation errors on the target time. The x-axis represents the fidelity between $\rho_{\rm error}$ and $\rho_{\rm qt}(\delta)$, and the y-axis represents the time difference required for $\rho_{\rm error}$ and $\rho_{\rm qt}(\delta)$ to evolve to a target angle of $2\pi/3$. The number of sampled points is 5000.

We performed Monte Carlo simulations (5000 runs) with $\delta = 0.15$, a representative value from our experiments, to evaluate the impact of $\eta_1, \eta_2, \phi_1, \phi_2$ on the target time. The results are shown in Fig. (S2).

When fidelity greater than 0.99, the target time bias is ± 0.025 (standard deviation of target time errors), indicating that state preparation errors introduce a small but quantifiable deviation from the ideal case. This result is consistent with the observed gap in Fig. 3(b) in the main text.

S7. COMPARISON BETWEEN SINGLE PHOTON STATES AND COHERENT STATES

In our experiment, we split a single photon into three path modes which give us a superposition state, $a|0\rangle + b|1\rangle + c|2\rangle$, and the mixed state is achieved by mixing $a|0\rangle + b|1\rangle + c|2\rangle$ and $a|0\rangle - b|1\rangle + c|2\rangle$ with probability p. Each mode corresponds to three energy levels of Hamiltonian $\hat{\mathrm{H}} = E_0|E_0\rangle\langle E_0| + E_1|E_1\rangle\langle E_1| + E_2|E_2\rangle\langle E_2|$. If we split a coherent state $|\alpha_t\rangle$ into three path modes, the prepared state will be a three-mode coherent state, $|\alpha_0\rangle|\alpha_1\rangle|\alpha_2\rangle$ with $\alpha_0 = a\alpha_t$, $\alpha_1 = b\alpha_t$ and $\alpha_2 = c\alpha_t$. The mixed states can also be viewed as the mixture of $|\alpha_0\rangle|\alpha_1\rangle|\alpha_2\rangle$ and $|\alpha_0\rangle|-\alpha_1\rangle|\alpha_2\rangle$ with probability p,

$$\rho_{classical} = p|\alpha_0\rangle\langle\alpha_0| \otimes |\alpha_1\rangle\langle\alpha_1| \otimes |\alpha_2\rangle\langle\alpha_2| + (1-p)|\alpha_0\rangle\langle\alpha_0| \otimes |-\alpha_1\rangle\langle-\alpha_1| \otimes |\alpha_2\rangle\langle\alpha_2|. \tag{11}$$

The evolution governed by the Hamiltonian $\hat{\mathrm{H}}$ will change the state $|\pm\alpha_i\rangle$ to $|\pm\alpha_i'\rangle = |\pm\alpha_i \exp(-iE_i t)\rangle$. We will omit the subscript *classical* of the initial state and replace it by ρ_0. The final state after the evolution is

$$\begin{aligned} \rho_t &= \exp(-i\hat{\mathrm{H}}t)\rho_0 \exp(i\hat{\mathrm{H}}t) \\ &= p|\alpha_0'\rangle\langle\alpha_0'| \otimes |\alpha_1'\rangle\langle\alpha_1'| \otimes |\alpha_2'\rangle\langle\alpha_2'| + (1-p)|\alpha_0'\rangle\langle\alpha_0'| \otimes |-\alpha_1'\rangle\langle-\alpha_1'| \otimes |\alpha_2'\rangle\langle\alpha_2'|. \end{aligned} \tag{12}$$

The Bloch angle Θ between the initial state and the final state can be calculated by

$$\cos\Theta(\rho_0, \rho_t) = \frac{d\mathrm{Tr}\,(\rho_0\rho_t) - 1}{\sqrt{(d\mathrm{Tr}\,(\rho_0^2) - 1)(d\mathrm{Tr}\,(\rho_t^2) - 1)}}. \tag{13}$$

From the fact that $\langle \alpha_i | \pm \alpha_i' \rangle = \exp(-|\alpha_i|^2(1 \mp \mathrm{e}^{-iE_it}))$ and $\mathrm{Tr}(|\alpha_i\rangle\langle \pm\alpha_i'|) = \exp(-|\alpha_i|^2(1 \mp \mathrm{e}^{-iE_it}))$, we can get

$$\begin{aligned} \mathrm{Tr}(\rho_0\rho_t) &= (p^2 + (1-p)^2)\left(\exp\left(-2|\alpha|^2(3 - \cos E_0t - \cos E_1t - \cos E_2t)\right)\right) \\ &\quad + 2p(1-p)\exp\left(-2|\alpha|^2(3 - \cos E_0t + \cos E_1t - \cos E_2t)\right), \\ \mathrm{Tr}(\rho_0^2) &= \mathrm{Tr}(\rho_t^2) = p^2 + (1-p)^2 + 2p(1-p)\exp(-4|\alpha|^2), \end{aligned} \tag{14}$$

where we set $\alpha_0 = \alpha_1 = \alpha_2 = \alpha$. The optimal state, based on the theory, to reach the OQSL is to set the factor $p = 1/2$. According to Eq. (13), the cosine value of the evolution angle is

$$\begin{aligned} &\cos\Theta_{classical} = \\ &\frac{1}{-2 + 3(1 + \exp(-4\alpha^2))}\{-2 + 3(\exp(-2\alpha^2(3 - \cos E_0t - \cos E_1t - \cos E_2t) + \\ &\exp(-2\alpha^2(3 - \cos E_0t + \cos E_1t - \cos E_2t))\}, \end{aligned} \tag{15}$$

which is different from the that of the optimal state in our work, $\cos\Theta_{op} = \cos((E_2 - E_0))t)$. The results are shown in Fig. (S3), where the parameters are set as $\alpha = 0.1$, $E_0 = 0$, $E_1 = 1$, $E_2 = 2$. From this figure, one can obviously find the results simulated by the classical light are different from our single-photon results.

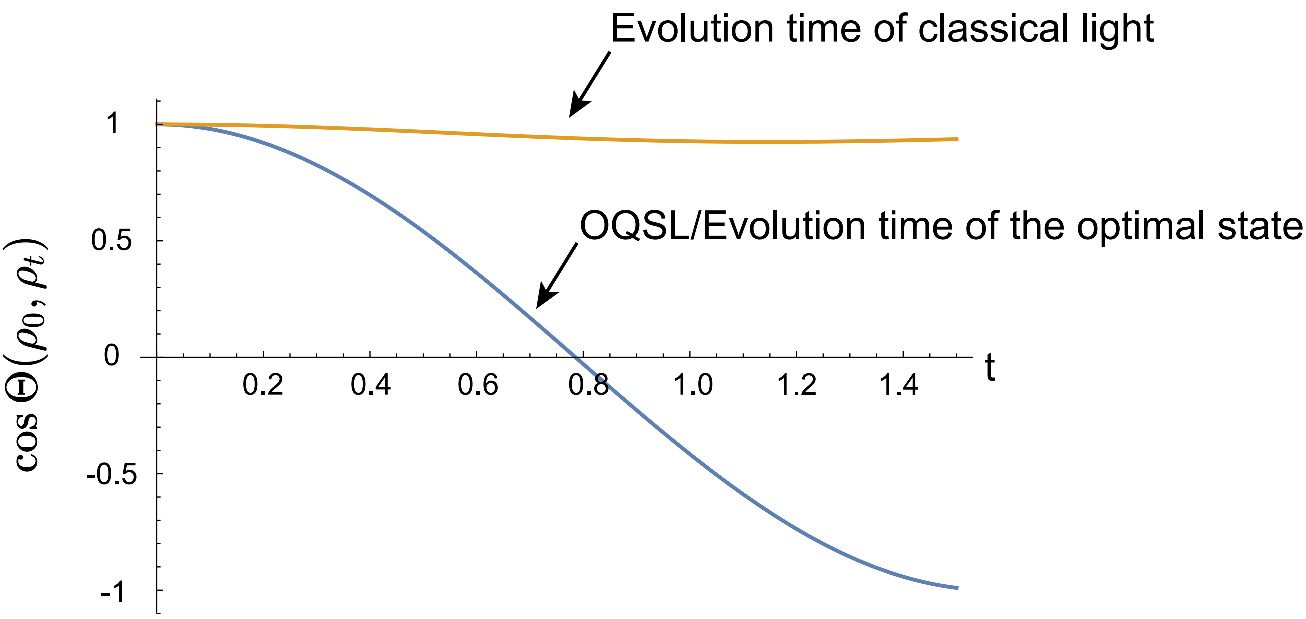

FIG. S3: The comparison between the OQSL and the result simulated by the classical light.

The only way to use coherent states to simulate our experiments is to post-select the one-photon component of the state during the measurement process. In that case, one can post-select $(|100\rangle \pm |010\rangle + |001\rangle)/\sqrt{3}$ in $|\alpha_0\rangle|\pm\alpha_1\rangle|\alpha_2\rangle$, which is equivalent to the single photon superposition state in our work mathematically. However, this post-selection comes at the expense of neglecting zero- and high-photon components, which is an artificial simulation by producing a statistical distribution similar to the quantum system. One can reproduce every quantum (even beyond quantum) statistical behavior with only classical inputs at a cost of more resources due to the reduced post-selection probability. Nevertheless, this approach cannot reflect the behavior of a true quantum system and cannot convincingly demostrate the OQSL in the experiment.

In conclusion, the utilization of a single-photon source in our work is both deliberate and well-justified for investigating the QSL in an N-level quantum system.

S8. DECOMPOSITION OF THE EVOLUTION

In our setup, we want to realize the unitary evolution $U(t) = \exp(-i\hat{H}t)$, where the Hamiltonian $\hat{H} = E_0|E_0\rangle\langle E_0| + E_1|E_1\rangle\langle E_1| + E_2|E_2\rangle\langle E_2|$. Any 3-dimensional Hamiltonian can be expressed as $\hat{H} = \sum_{i=1}^{8} c_i\hat{\lambda}_i + c_0 I$, where $\hat{\lambda}_i$ is the i-th generator of SU(3), namely the Gell-Mann matrix, and I is the identity. We can determine the coefficients of the Hamiltonian prepared in our experiment that

$$\hat{H} = c_0 I + c_7\hat{\lambda}_7 + c_8\hat{\lambda}_8, \tag{16}$$

where $c_0 = (E_0 + E_1 + E_2)/3$, $c_7 = (E_0 - E_1)/2$, $c_8 = \sqrt{3}(E_0 + E_1 - 2E_2)/6$ and $\hat{\lambda}_7 = diag[1, -1, 0]$, $\hat{\lambda}_8 = diag[1, 1, -2]/\sqrt{3}$. Due to the fact that $[\hat{\lambda}_7, \hat{\lambda}_8] = [\hat{\lambda}_7, I] = [\hat{\lambda}_7, I] = 0$, the unitary evolution can be decomposed into

$$\begin{aligned} U(t) &= \exp(-i\hat{H}t) = \exp(-i(c_0 I + c_7\hat{\lambda}_7 + c_8\hat{\lambda}_8)t) \\ &= \exp(-ic_0 It)\exp(-ic_7\hat{\lambda}_7 t)\exp(-ic_8\hat{\lambda}_8 t). \end{aligned} \tag{17}$$

Because of the commutativity of the three observables, we can use cascaded phase shifts to perfectly simulate the evolution process.

Actually, the unitary evolution can be easily simulated by the cascaded waveplates in three optical paths, because the three path modes of single photons are viewed as the eigenstates of the Hamiltonian in our experiment. The evolution can just been simulated by adding phase shifts in each path, which leads to $\phi_i = E_i t$.

For spontaneous emission system, the analytical solution to the spontaneous equation can be expressed as

$$\rho(t) = e^{-iHt}(K_0(t)\rho(0)K_0^\dagger(t) + K_1(t)\rho(0)K_1^\dagger(t))e^{iHt}, \tag{18}$$

where $H = -\frac{1}{2}\omega_0\lambda_z$ and ω_0 represents the energy gap between the ground state $|0\rangle$ and the excited state $|1\rangle$. K_i is the Kraus representation of amplitude damping channel. The expressions of these two operators are

$$K_0 = \begin{pmatrix} 1 & 0 \\ 0 & \sqrt{1-p} \end{pmatrix}, \qquad K_1 = \begin{pmatrix} 0 & \sqrt{p} \\ 0 & 0 \end{pmatrix}, \tag{19}$$

where $p = 1 - e^{-\gamma t}$ represents the probability of $|1\rangle$ that decays to $|0\rangle$ and γ describes the rate of spontaneous emission. Therefore, we can simulate the time evolution of a spontaneous emission system by implementing a amplitude damping channel and a unitary evolution separately. It is noteworthy that these two evolution processes commute. Specifically, for a general quantum state

$$\rho = \begin{pmatrix} a & b \\ c & d \end{pmatrix} \tag{20}$$

we have

$$\begin{aligned} K_0 U(t)\rho U^\dagger(t) K_0^\dagger + K_1 U(t)\rho U^\dagger(t) K_1^\dagger &= U(t)(K_0\rho K_0^\dagger + K_1\rho K_1^\dagger)U^\dagger(t) \\ &= \begin{pmatrix} a + pd & \sqrt{1-p}e^{-i\omega_0 t}b \\ \sqrt{1-p}e^{i\omega_0 t}c & (1-p)d \end{pmatrix} \end{aligned} \tag{21}$$

* Electronic address: liangxu.ceas@nju.edu.cn
† Electronic address: jing.liu@hainanu.edu.cn
‡ Electronic address: lijian.zhang@nju.edu.cn

[1] J. Altepeter, E. Jeffrey, and P. Kwiat (Academic Press, 2005) pp. 105–159.